Current Biology 22, 668–675, April 24, 2012 ©2012 Elsevier Ltd All rights reserved DOI 10.1016/j.cub.2012.02.065

Article

Free Extracellular Diffusion Creates the Dpp Morphogen Gradient of the *Drosophila* Wing Disc

Shaohua Zhou,[1,4] Wing-Cheong Lo,[2,4] Jeffrey L. Suhalim,[1,3,4] Michelle A. Digman,[3,4,5] Enrico Gratton,[3,4,5] Qing Nie,[2,3,4] and Arthur D. Lander[1,3,4,*]

[1]Department of Developmental and Cell Biology
[2]Department of Mathematics
[3]Department of Biomedical Engineering
[4]Center for Complex Biological Systems
[5]Laboratory for Fluorescence Dynamics
University of California, Irvine, Irvine, CA 92697, USA

Summary

Background: How morphogen gradients form has long been a subject of controversy. The strongest support for the view that morphogens do not simply spread by free diffusion has come from a variety of studies of the Decapentaplegic (Dpp) gradient of the *Drosophila* larval wing disc.

Results: In the present study, we initially show how the failure, in such studies, to consider the coupling of transport to receptor-mediated uptake and degradation has led to estimates of transport rates that are orders of magnitude too low, lending unwarranted support to a variety of hypothetical mechanisms, such as "planar transcytosis" and "restricted extracellular diffusion." Using several independent dynamic methods, we obtain data that are inconsistent with such models and show directly that Dpp transport occurs by simple, rapid diffusion in the extracellular space. We discuss the implications of these findings for other morphogen systems in which complex transport mechanisms have been proposed.

Conclusions: We believe that these findings resolve a major, longstanding question about morphogen gradient formation and provide a solid framework for interpreting experimental observations of morphogen gradient dynamics.

Introduction

Biological pattern formation is often orchestrated by morphogens, molecules that, when released at discrete locations, form concentration gradients from which cells obtain positional information. The idea that such gradients form by simple diffusion was advocated by Crick, based on observed constraints on gradient sizes [1], and many quantitative models of morphogen gradients assume this mechanism (e.g., [2–7]). It has been argued, however, that some experimental results are inconsistent with diffusive transport of extracellular morphogens [8–11], and theoretical objections have been raised against free diffusion for not being sufficiently robust [12] or controllable [13].

Attempts to resolve this controversy by following the behaviors of fluorescently tagged morphogens have yielded conflicting results. In the *Drosophila* larval wing imaginal disc, studies with labeled Decapentaplegic (DppGFP) suggested a transport coefficient of 0.1 $\mu m^2\ sec^{-1}$, two orders of magnitude too slow for free diffusion [9]. Such measurements lend support to the view that morphogens move by active mechanisms such as serial transcytosis (i.e., repeated rounds of endo- and exocytosis [12]), travel along or within specialized filopodia [14, 15] or by "restricted" diffusion, in which transport involves transfers between immobile sites in the extracellular matrix [16]. In contrast, in the zebrafish neural tube, studies of fluorescently tagged fibroblast growth factor 8 (Fgf8) have yielded much faster transport rates, (D = 50–90 $\mu m^2\ sec^{-1}$), consistent with simple, free diffusion in the extracellular space [17]. With the cytoplasmic morphogen Bicoid, which forms a gradient in the syncytial *Drosophila* embryo, different approaches have led to estimates of transport coefficients ranging from as low as 0.3 to as high as 7 $\mu m^2\ sec^{-1}$ [18–20].

Although it has been suggested that different morphogens move by different mechanisms or that different transport processes operate over short versus long distances [17, 19, 21, 22], we wondered whether some of the perceived variability in morphogen transport behavior might reflect the misinterpretation of data, and not real biological differences. Here we present evidence in support of this view, based upon observations and analysis of the Dpp gradient of the *Drosophila* wing disc. We believe this work lays to rest longstanding controversies about Dpp transport and suggests ways in which to guide future inquiry into the transport of morphogens in general.

Results

We note that most reports claiming to provide strong evidence for morphogen transport at rates much slower than free diffusion have utilized the method of fluorescence recovery after photobleaching (FRAP). For example, Kicheva et al. [9], and Gregor et al. [18], used the kinetics of FRAP—i.e., the rate of recovery of a photobleached zone—to estimate spreading rates for DppGFP and BicoidGFP, as 0.1 $\mu m^2\ sec^{-1}$ and 0.3 $\mu m^2\ sec^{-1}$, respectively. Typically, when deriving transport rates from FRAP kinetics, one assumes that transport is the only process upon which accumulation of observed molecules during the observation time depends. This assumption is often not stated explicitly but is critical: if other processes, such as binding to immobile sites, or degradation, occur on the time scale of observation, FRAP kinetics can be dominated by these processes and may contain little information about transport. Although an extended treatment of this issue is provided elsewhere (see Supplemental Experimental Procedures available online), a simple illustration makes the point: here we consider two mathematical models of morphogen gradient formation in a *Drosophila* wing disc. In one, transport occurs by an inherently slow process (e.g., transcytosis), at the rate reported by Kicheva et al. [9], i.e., D = 0.1 $\mu m^2\ sec^{-1}$. In the other, morphogen molecules move by fast, unhindered, extracellular diffusion (D = 20 $\mu m^2\ sec^{-1}$) but are subjected to receptor-mediated uptake, internalization, and degradation (using rate constants consistent with the Dpp gradient length-scale normally observed in late larval wing discs [23]).

Figure 1 shows the expected kinetics of recovery after photobleaching, according to the two models. Despite having

*Correspondence: adlander@uci.edu

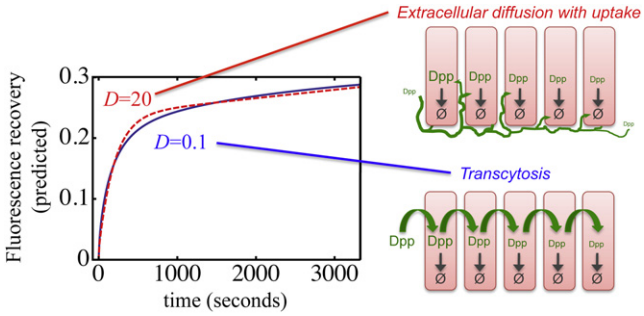

Figure 1. Fluorescence Recovery after Photobleaching Can Provide Little or No Information about Transport

In models of morphogen transport by extracellular diffusion with cellular uptake, accumulation, and degradation, if diffusion is fast enough, overall FRAP kinetics will tend to reflect the time scale of degradation, not transport. This is illustrated by simulating the expected results of FRAP within a 10 μm-wide stripe adjacent to the source of the morphogen Dpp in the *Drosophila* wing disc according either to a model of transcytotic transport (blue) with an effective diffusion coefficient of 0.1 $\mu m^2\ sec^{-1}$ [9] or a model based on free extracellular diffusion with uptake (red, dashed), with a diffusion coefficient of 20 $\mu m^2\ sec^{-1}$. For further details, see Supplemental Information.

transport rates 200-fold apart, they predict nearly indistinguishable FRAP behavior. The reason is that, in the model that assumes slow transport, FRAP kinetics are dominated by the transport rate, whereas in the model that assumes fast, diffusive transport, the kinetics are dominated by the morphogen degradation rate, and are essentially independent of transport. Thus, one cannot derive a transport rate from a FRAP experiment of the type shown, unless one has already assumed a priori that transport is not fast. Generally speaking, situations in which FRAP kinetics will fail to provide useful information about transport rate are those in which two conditions are met: transport is fast relative to the time and length scale of observation, and degradation is sufficiently slow that, at steady state, the amount of morphogen accumulated on and within cells is much larger than the amount freely diffusing in the extracellular space.

Are these conditions met by Dpp in the wing disc? Calculations suggest that they easily could be. First, if Dpp were to move by free diffusion ($D \geq 10\ \mu m^2\ sec^{-1}$), one would expect it to traverse distances of ~30 μm (the typical maximum distance over which FRAP is performed in the wing disc) in ≤ 20 s, much shorter than typical FRAP observation times (tens of minutes). Second, from fluorescent images it has been estimated that >85% of the Dpp in wing discs is inside cells [9, 24]. Of the remainder, the amount free in the extracellular space (as opposed to being bound to cell-surface molecules) cannot be determined from images but may be estimated, given recent measurements of absolute DppGFP concentrations (~800 molecules/μm^2 near the Dpp source [9]), estimates of the extracellular volume fraction [2], and the reasonable assumption that free extracellular Dpp does not greatly exceed the effective dissociation constant of its receptor (see Supplemental Information). Based on this information, one can calculate that free extracellular Dpp is unlikely to account for more than 3% of the total morphogen and less than 1% of that which is normally visualized by fluorescence imaging (see Supplemental Information; note that this calculation makes no assumptions about transport mechanisms).

It may seem counterintuitive that the free diffusion of such a small fraction of total morphogen can support the formation of the entire Dpp gradient, but it is precisely when diffusion is fast that this is so. In effect, a scarcity of extracellular Dpp, rather than arguing against transport by diffusion, as others have suggested [9], is just what free diffusive transport predicts (see Supplemental Experimental Procedures, section 1.2).

How then might one determine, experimentally, whether morphogen transport occurs by free diffusion or some slow process such as transcytosis or "restricted" diffusion? Here we apply four approaches to the Dpp gradient of the wing disc: fluorescence spreading after photoactivation, spatial FRAP, fluorescence correlation spectroscopy (FCS), and pair correlation function microscopy. In each case, the results support transport by free, extracellular diffusion.

Photoactivation relies upon the ability to tag molecules with probes that can be rendered abruptly fluorescent with brief pulses of light, and it has been used as a means to follow proteins within cells [25]. We fused Dpp to Dendra2, which switches from green fluorescence to red after exposure to UV light [26] and expressed it in the normal Dpp expression domain of the wing disc. DppDendra2 formed gradients along the anteroposterior axis similar to those observed with Dpp tagged with GFP [8, 24] or other moieties [27]; it also turned on Dpp target genes at appropriate locations (Figure S1; Experimental Procedures). Like DppGFP [8, 9, 24], DppDendra2 was mainly found in punctuate intracellular accumulations in the most apical 5 μm of the columnar disc epithelial cells. We carried out FRAP experiments with DppDendra2 and obtained results similar to those reported for DppGFP [9]: recovery on a timescale of 10–15 min and a large "immobile fraction" (non-recovering or very slowly recovering fraction; Figure S1).

Thus, in all regards tested, DppDendra2 behaved like other tagged forms of Dpp in the wing disc. Yet when regions within the DppDendra2 gradient were photoactivated and followed, no obvious spreading of red fluorescence was seen. To increase the ability to detect spreading, we photoactivated pairs of stripes 10 μm apart and looked in the region between them; still no significant spreading was evident, either on short or long time scales (min to hr; Figures 2A–2O, Figure S2A and S2B). To further improve sensitivity, we prebleached a large region within the DppDendra2 gradient, waited 30 min for fluorescence recovery, then photoactivated within this region (prebleaching removes background fluorescence due to "immobile fractions"). Even then, fluorescence spreading after photoactivation was undetectable (Figure S2). To control for the possibility that background autofluorescence, fluctuating laser power, sample movement, or other such artifacts might mask small amounts of spreading, we also followed the intracellular puncta of photoactivated DppDendra2 at high magnification and observed no obvious increases in the numbers or sizes of such accumulations next to photoactivated regions over a 30 min interval (Figure S2).

The explanation for these results cannot be that fusion to Dendra2 prevents Dpp transport, because DppDendra2 molecules formed a normal morphogen gradient and behaved similarly to DppGFP in FRAP studies (Figure S1). It also seemed unlikely that photoactivation per se interfered with the transport of DppDendra2 molecules, given the relatively low energy of laser light used. However, to control for this possibility, we fused Dendra2 to another morphogen, Wingless. When expressed and photoactivated in the wing disc, spreading of a significant fraction of Wg-Dendra2 fluorescence was observed (Figures 2P–2Z).

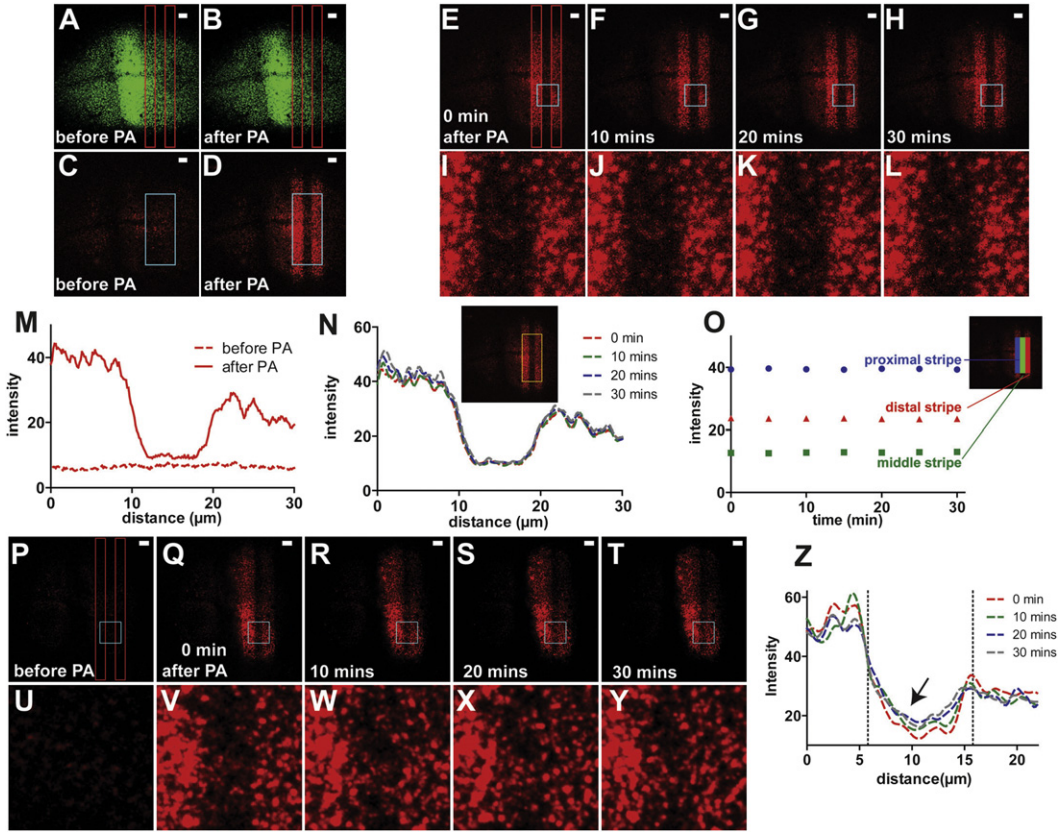

Figure 2. Lack of Spreading of Photoactivated DppDendra2

(A–D) Confocal images of a DppDendra2-expressing wing disc before and after photoactivation (PA). Before PA, bilaterial exponential gradients are observed along the horizontal (anteroposterior axis) in the green channel (A) with minimal red signal (C). PA was carried out in two rectangular regions (red boxes in A and B) using a 20 μsec pulse of 405 nm light, producing two red fluorescent stripes (D).

(E–H) Images after PA. Five optical slices covering the apical part of the disc were taken at 5 min intervals for 30 min, maximum projected, and intensity profiles calculated (similar results were obtained when optical slices were summed, instead of maximum projected). Cyan boxes in (E)–(H) are magnified in (I)–(L)

(M) Average intensity along the vertical (dorsoventral axis) is plotted along the horizontal axis of the cyan box in (C) and (D).

(N) Intensity profiles along the horizontal axis of the yellow box (see inset) at times after PA.

(O) Average intensities inside the proximal (near the morphogen source) and distal PA-stripes, and the region lying between them ("middle stripe"), at different times. The proximal, middle, and distal stripes correspond to the blue, green, and red regions in the inset.

(P–Z) Spreading of photoactivated WinglessDendra2. (P)–(T) are time-lapse images from a wing disc expressing WinglessDendra2 in the Dpp domain (dpp-gal4/UAS-WinglessDendra2) and photoactivated and imaged as in (A)–(D).

(U–Y) Magnified views of the cyan boxes in (P)–(T).

(Z) Intensity profiles along the horizontal axis of each cyan box were plotted at different time points. Dashed lines mark the boundaries of the two photoactivated regions. Note significant spreading of fluorescence (arrow). In addition, in DppDendra2-expressing discs in which the entire disc (including the production region) was photoactivated, except for a small stripe, we also observed some spreading of fluorescence into the nonphotoactivated region (data not shown). Scale bars in (A)–(H) and (P)–(T) represent 10 μm.

The lack of detectable spreading of photoactivated Dpp is predicted by models of transport by free extracellular diffusion because, in such models, only a small fraction of total Dpp participates in transport; the vast majority is trapped permanently on or within cells. In contrast, under the model of transport by transcytosis, 30% of total Dpp must be moving from cell to cell to fit FRAP data (this rises to 60%–70% in the case of a freshly recovered prebleached region, as in Figure S2). Under such conditions, spreading after photoactivation should be quite obvious, peaking at ~5 min after photoactivation (see Supplemental Information). Note that similar predictions are also made by the "restricted extracellular diffusion" model, because it is the slow rate of transport per se and not the particular model that necessitates such behavior (see Supplemental Information).

As a second approach for assessing the means of Dpp transport, we used "spatial FRAP," in which fluorescence recovery is followed as a function of location within a photobleached region. Even when overall FRAP kinetics are dominated by processes other than transport, differences in recovery times at different distances from a bleach boundary can potentially provide a measure of transport rate (see Supplemental Experimental Procedures). Kicheva et al. [9] presented, as supplemental data, several spatial FRAP experiments for DppGFP in the wing disc and fit the results to the predictions of a transcytosis model. However, their experiments were not designed to distinguish among transport models and, in most cases, were carried out using geometries in which both fast (e.g., free extracellular diffusion) and slow (e.g., transcytosis or restricted diffusion) models could still fit

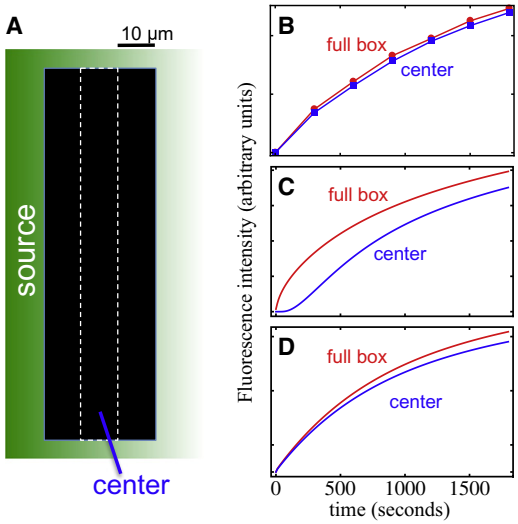

Figure 3. Results of Spatial FRAP Support Transport by Rapid Diffusion

Whereas the kinetics of FRAP within a single photobleached region cannot necessarily distinguish between slow and fast transport (see Figure 1), it should be possible to do so by comparing FRAP kinetics at different locations within a photobleached region. As diagrammed in (A), a 30 × 150 μm-wide rectangle was photobleached in the posterior compartment of a DppDendra2-expressing wing disc and observed at multiple locations for 30 min. Fluorescence intensities, corrected for bleach depth, were measured for the entire box, as well as for a 10 × 150 μm region in the center of the box. The results of a typical experiment are shown in (B). The predictions of models based on transcytosis (D = 0.1 $\mu m^2\ sec^{-1}$) and free extracellular diffusion (D = 20 $\mu m^2\ sec^{-1}$) are shown in (C) and (D), respectively. Note the significant time displacement (~250 s) between the two curves required by the transcytosis model (C; similar behavior would be produced by slow, restricted extracellular diffusion). The delay corresponds to the time required for a molecule with D = 0.1 $\mu m^2\ sec^{-1}$ to travel 10 μm.

the data. The optimal configuration for distinguishing among models is one in which two sites are observed, such that fluorescence recovery at one requires prior transport through the other. This can be achieved by bleaching a large rectangle and comparing recovery in its center with recovery in the rectangle as a whole. When we did this with DppDendra2-expressing wing discs, the lack of significant delay in central recovery (Figure 3) implied a rate of transport far faster than 0.1 $\mu m^2\ sec^{-1}$.

If such fast transport is truly due to free extracellular diffusion, we ought, in principle, to be able to observe it directly. Although freely diffusing Dpp molecules are expected to be rare (on the order of eight molecules or less per μm^2, given the calculations mentioned previously), their existence should be detectable by FCS, which is effectively a single-molecule method. FCS uses fluctuations in signal intensity to measure average residency times of fluorescent molecules within a small (~1 fL) volume illuminated by a laser beam. Because intercellular spaces in the wing disc are too narrow to resolve by light microscopy, we labeled plasma membranes with the vital dye FM4-64 and used its fluorescence to focus the laser at sites of cell-cell contact (Figure 4A).

When FCS was performed on discs expressing DppDendra2, the data were well fit by a two-species model, in which 65% of the autocorrelation signal comes from molecules that diffuse rapidly (D = 21 ± 3 $\mu m^2\ s^{-1}$) and 35% from ones that move much more slowly (D = 0.03 ± 0.006 $\mu m^2\ s^{-1}$) (green triangles in Figure 4B). Similar results were obtained in discs expressing DppGFP (Figures 4C and 4D). The fast diffusion coefficients obtained in these experiments are appropriate for a freely soluble protein in extracellular space. The slower diffusion coefficients are consistent with Dpp bound to proteins of the plasma membrane (e.g., receptors, glypicans [27, 28]). Interestingly, when FCS experiments were repeated in discs mutant for the glypican dally, which has been suggested to play a major role in shaping the Dpp gradient [11, 27, 28], we observed only a small change in the relative contributions of fast and slow moving species (Figure S3), suggesting that the slowly moving pool is not primarily composed of dally-bound Dpp. As a negative control, we also expressed a GFP-tagged transmembrane protein, cd8, in the wing disc and measured its diffusivity. Consistent with expectations for an integral membrane protein, only a single, slow diffusion coefficient was observed (0.05 ± 0.003 $\mu m^2\ s^{-1}$; gray crosses in Figure 4B).

The calculation of transport parameters from FCS depends upon assumptions that can be difficult to validate in complex tissues (e.g., knowledge of the size and shape of the illuminated volume). To measure diffusivity independent of such assumptions, we also used a new method, pair correlation function (pCF) microscopy [29–31]. In pCF, fluorescence is followed at two points. The time required for fluctuations at one point to arrive at the other provides a direct measure of transport rate, independent of the details of the fluctuations themselves. Figures 4E–4G show the results of pCF, in a DppDendra2-expressing wing disc, in which the points were 5 pixels apart, along a border between two cells. Cross-correlation demonstrated the existence of a population of fluorescent molecules that take 5.1 ± 1.1 ms to traverse 0.525 μm. This corresponds to an effective diffusion coefficient of 21 ± 4 $\mu m^2\ sec^{-1}$, essentially identical to the one measured by FCS (Figure 4D). As evidence that such cross-correlations truly represent transport, when observations were made at one point on a border between two cells and a second point inside one of the cells, positive cross-correlation was not seen (Figure S4).

Discussion

The results described above strongly support the view that the Dpp gradient of the *Drosophila* wing disc forms by free, extracellular diffusion, coupled with uptake by cell-surface receptors and subsequent degradation. It is precisely because transport is fast, relative to uptake and degradation, that fluorescence recovery kinetics in a simple FRAP experiment fail to provide information about transport. It is also precisely because transport is fast that very little Dpp needs to be in the transported pool (i.e., free in the extracellular space). Indeed, in the wing disc, Dpp molecules actually undergoing transport may be sufficiently rare that only methods with single-molecule sensitivity, such as FCS and pCF microscopy, can reliably detect them.

Although the experimental data presented here focus on the Dpp gradient of the wing disc, other morphogen systems likely face similar issues. For example, the fact that measurements of Bicoid transport in the early *Drosophila* embryo by FRAP [18, 20] yield values 8–23 times smaller than measurements by FCS [19], could be explained by reversible binding of Bicoid to immobile structures (e.g., cytoskeletal components, organelles). FRAP kinetics might then reflect the dissociation rate from such structures, rather than Bicoid transport (see Supplemental Information).

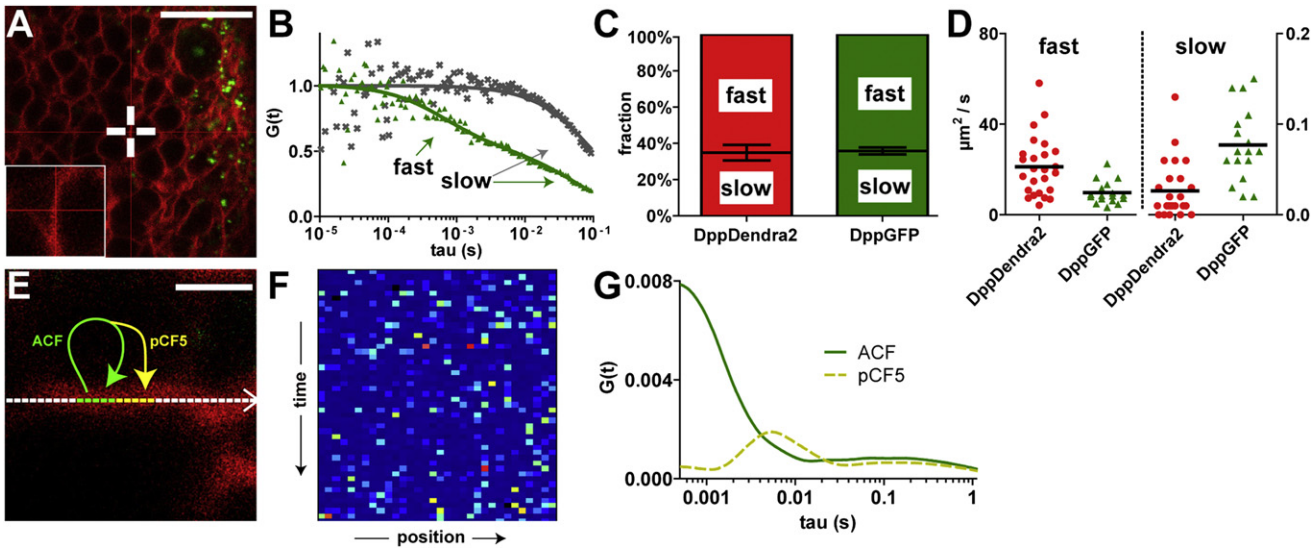

Figure 4. Measuring Extracellular Diffusion of Dpp

(A) Confocal images of DppDendra2-expressing wing discs used for FCS (green, DppDendra2; red, FM4-64 to label cell membranes). Cross-hairs mark location of FCS measurement. Inset shows a magnified view. Scale bar represents 10 μm.

(B) Autocorrelation curves for DppDendra2 (green) and a membrane-anchored control, cd8GFP (gray; expressed under the control of dpp-Gal4). Data from DppDendra2 fit a two-component diffusion model with fast and slow components.

(C) Proportions of molecules in fast and slow pools measured for DppDendra2 (as in B) and DppGFP (data not shown). Error bars represent SEM.

(D) Calculated diffusion coefficients. Each point represents an independent measurement at a different location in a total of 11 wing discs for DppDendra2 and 4 wing discs for DppGFP. Averages (black bars) were 21 ± 3 $\mu m^2\ sec^{-1}$ and 0.03 ± 0.006 $\mu m^2\ sec^{-1}$ for DppDendra2 and 10 ± 1 $\mu m^2\ sec^{-1}$ and 0.08 ± 0.01 $\mu m^2\ sec^{-1}$ for DppGFP (values are means ± SEM).

(E) pCF microscopy was carried out by repeatedly scanning a 3.2 μm-long line along a site of cell contact in a DppDendra2-expressing disc (stained as in A). Scale bar represents 1 μm. Fluorescence intensities were converted to an intensity carpet (F) in which the horizontal and vertical directions represent position and time, respectively, and intensity is color-coded. Autocorrelation, calculated at each location and averaged over all locations, was plotted (ACF) in (G). For pair correlation, fluctuations in each of 5 pixels (depicted in green along the line in E) were each cross-correlated with pixels five positions to the right (depicted in yellow in E), and the correlation curves averaged and plotted (pCF5). The position of the peak in the pCF5 curve corresponds to the average time delay required for DppDendra2 to move 5 pixels.

Recently, Schwank et al. [16] used genetic manipulations to show that the spread of Dpp in the wing disc does not require its receptor, thickveins (Tkv), thereby arguing against transport through receptor-mediated transcytosis. Although they acknowledged that such data do not rule out other forms of transcytosis, they favored a "restricted extracellular diffusion" model, in which Dpp transport occurs through periodic binding and unbinding from immobile sites in the extracellular matrix. In support of this, they cited the slow Dpp transport kinetics inferred by Kicheva et al. [9], but as we have seen here, those data only imply slow transport if one has already assumed that transport is slow. They also cited the observation that a secreted form of GFP fails to form a gradient in wing discs [8] as evidence that efficient, free extracellular diffusion cannot occur, but this observation is more likely explained by the fact that GFP, with nothing to bind to, simply diffuses through and out of the wing disc so fast that no stable gradient can be formed. Finally, Schwank et al. [16] point to a growing body of literature suggesting that proteoglycans—glypicans in particular—control the formation of the Dpp gradient [11, 27, 28, 32–35], as evidence against transport by free extracellular diffusion.

The data presented here, however, lend no support to the idea of "proteoglycan-restricted" Dpp transport. Reversible binding of a large proportion of transported Dpp to glypicans (which, incidentally, are components of the cell surface, not the extracellular matrix) should have produced results in photoactivation and spatial FRAP experiments similar to those predicted by transcytosis models and very different from what was observed (Figures 2 and 3; see Supplemental Information). Moreover, FRAP studies on dally mutant discs suggested that the proportion of mobile Dpp in the extracellular environment that is dally-bound is not particularly large (Figure S3).

How can these results be reconciled with the growing body of literature suggesting an important role for proteoglycans in gradient formation, not only for Dpp but also for many other morphogens (e.g., [11, 27, 28, 32–41])? To date, all experiments that have implicated proteoglycans in morphogen gradient formation have focused either on changes that occur in the distributions of total morphogen protein or in morphogen activity (a function, presumably, of receptor occupancy). As discussed above, whenever transport occurs by free, rapid, extracellular diffusion, with only a small fraction of total morphogen being transported, the dynamics of the total and receptor-associated morphogen pools need not bear any relationship to transport rate. Rather, those dynamics will usually reflect processes downstream of and slower than transport, such as binding, internalization, and degradation. It is, in fact, possible to attribute all known results of proteoglycan manipulation on morphogen gradient formation to effects on such downstream processes, especially given that proteoglycans not only bind morphogens, but they also influence the formation and stability of morphogen-receptor complexes [42].

Overall, the work presented here supports the simplest of models for morphogen transport: free diffusion in the

extracellular space, hindered only by the viscosity of the extracellular fluid and the tortuosity of intercellular paths [43]. In some morphogen gradient systems, reversible binding to immobile molecules may also slow effective transport, but for Dpp in the wing disc, no evidence of such an effect was obtained.

An important lesson to be gleaned from the present work is that morphogen gradients cannot generally be treated in the singular, because they are usually composites of coupled gradients in multiple compartments (e.g., free, surface-bound, intracellular, etc.). Even when they have similar steady-state shapes, such gradients can evolve very differently in time. For Dpp, the difference in dynamics between transported and stationary pools is evidently great, but this may not always be so. In cases in which morphogen-receptor affinities are low (so that free extracellular concentrations need to be high), and there is little build-up of internalized morphogen receptor complexes, total morphogen dynamics might indeed reflect those of the molecules undergoing transport. The Fgf8 gradient of the zebrafish neural tube probably falls into this category, because large intracellular accumulations of morphogen are not seen in neural tube cells [17] and the affinity of Ffg8 for its receptors is notably weak (0.1–1 μM [44]). Not surprisingly, all observations of gradient dynamics in that system, whether by genetic manipulation or direct measurement (e.g., FCS), have consistently supported a simple model of extracellular diffusion coupled to receptor-mediated uptake [17, 45].

Experimental Procedures

Fly Strains and Transgenes

Flies were from Bloomington Drosophila Stock Center unless noted. DNA encoding Dendra2 was fused to *Dpp* and *Wingless* (*Wg*) complementary DNA using a strategy similar to that described for DppGFP and WgGFP [8, 46]: *Dendra2* was cloned into an AvrII site introduced into *Dpp* between amino acids D485 and T486. Similarly, *Dendra2* was inserted into an AvrII site introduced into *Wg* between W38 and W39. Both sequences were subcloned into pUAST or pUASTattB, and transgenic flies were generated by either P element-mediated transformation or PhiC31-mediated transformation [47]. UAS-DppGFP transgenic flies were previously described [8, 24]. Expression was driven using the dpp-gal4 driver. Quantitative imaging (see below) showed that Dpp-Dendra2 formed exponential gradients in the anterior and posterior compartments of the wing disc, with an average length scale of 21 ± 1.5 μm in the posterior compartment. To assay for functional rescue by Dpp-Dendra2, we crossed dpp^{d12}/CyO, Act-GFP; dpp-gal4/TM6B flies to dpp^{d14}/CyO, Act-GFP; UAS-DppDendra2 flies. The dpp^{d12}/dpp^{d14}; dpp-gal4/UAS-DppDendra2 larvae were identified by lack of ubiquitous GFP and TM6B. The dpp^{d12}/dpp^{d14}; TM6B/UAS-DppDendra2 larvae served as a control.

Antibodies and Immunostaining

Wing discs were fixed in 4% formaldehyde for 15 min at room temperature, incubated with anti-spalt antibody (1:800; gift of Kavita Arora) at 4°C overnight, and then incubated with Alexa 555-Goat anti-rabbit (1:1,000, Invitrogen) at room temperature for 1.5 hr.

Imaging

Wing discs were dissected from third-instar larvae in M3 medium, and transferred to Clone-8 medium (Shields and Sang M3 [Sigma #S3652], with 10 μg/ml insulin [Sigma #I9278], 2% heat-inactivated fetal bovine serum, and 2.5% fly extract [48]) for time-lapse imaging. A channel was built on a glass slide with strips of magic tape (3M), filled with 60 μl Clone-8 medium, covered with a No. 1.5 coverslip (Corning), and sealed with rubber cement. Photobleaching and photoactivation were carried on a Fluoview1000 laser scanning confocal microscope (Olympus) with a 60×/1.2NA UPLSAPO water objective. DppDendra2 was excited with 488 nm Argon laser and detected with a 505–540 band-pass filter for the green channel and a 575–675 band-pass filter for the red channel. The following settings were used for most imaging: 1% laser power for 488 nm, 10% laser power for 558 nm, 12 bit, photon counting mode, sequential scan mode, 2 μs pixel dwell time, 1,024 × 1,024 pixels, 1.4 zoom, 0.147 μm × 0.147 μm pixel size, 2.7 μm optical slice thickness. The machine was turned on 30 min before use, allowing the system to stabilize. During imaging, samples were maintained at 25°C by a controller. Photobleaching was achieved with a 488 nm laser at 100% power with a 100 μs pixel dwell time at seven z positions. Photoactivation was achieved using a 405 nm laser at 10% power and a 20 μs pixel dwell time at single z position. During the chase period, the focal plane was maintained by a Zero-Drift Correction system (Olympus), and time points were taken at 5 min intervals. At each time point, a stack of five overlapping (2.7 μm thick) optical sections was collected, each 1 μm apart from the next, covering the most apical part of the columnar cell layer of the disc.

Controls were carried out (Figure S5) to demonstrate, under normal imaging conditions, a lack of significant photobleaching during imaging; a lack of dye saturation; a lack of detector saturation; and a linear relationship between Dendra2 concentration and fluorescence intensity. As in [9], controls also demonstrated that photobleaching occurred throughout the entire apicobasal depth of the wing disc (data not shown).

Data Analysis

Images were imported into ImageJ (National Institutes of Health [NIH]). Typically, a maximum projection of the z stack was done at each time point. The mean intensity of an arbitrary region outside the wing disc was used as background, and subtracted from ROIs (regions of interest). For photobleaching, subtraction was also used to correct for bleach depth (incomplete bleaching). In photoactivation studies, it was often noticed that total fluorescence (summed over the entire image) was not constant over time but in some cases underwent a gradual, linear increase (of up to 20% in rare cases) over the course of 1 hr. Control experiments suggested that this effect may have had to do with changes in disc thickness or rearrangement of the locations of fluorescent puncta to more apical locations, which are detected more efficiently. Because of this effect, photoactivation data were typically analyzed after normalization to total red fluorescence of the entire imaged area (or of a subregion of the imaged area containing most of the red signal).

Fluorescence Correlation Spectroscopy and Pair Correlation Function Microscopy

For FCS, wing discs were mounted in Ringer solution to minimize autofluorescence. Single point FCS was performed using either a Zeiss LSM510 Meta and Confocor3 system with a C-Apochromat 40×/1.20 NA water immersion objective or a Zeiss LSM710 system with a C-Apochromat 63×/1.20 NA water immersion objective. Measurements were performed in the apical part of the disc at room temperature. Each Confocor3 measurement lasted 100 s. Each LSM710 measurement lasted about 75 s. Normally, ten different locations were measured for each disc. Pixels were subjected to a 1 s prebleach at 100% laser power just prior to each measurement, to reduce contributions from immobile fluorophores. Data were analyzed with Confocor3 software or SimFCS (Laboratory for Fluorescence Dynamics, UC Irvine). Pair correlation function microscopy (pCF) was done with the SimFCS software and the LSM710 system. Data were collected using the line scan mode with pixel size 105 nm, pixel dwell time 6.3 μs, line time 471 μs, and 100,000 lines with 32 pixels per line.

Use of Prephotobleaching to Suppress Immobile Background Due to a Slowly Recovering Pool

As reported by Kicheva et al. [9] for DppGFP and confirmed here for DppDendra2 (Figure S1), recovery of Dpp fluorescence after photobleaching plateaus within the first hr at about 15%–30% of initial fluorescence. The existence of a large nonrecovering background ("immobile fraction") potentially reduces the sensitivity with which one can follow the dynamics of changes in fluorescence. In some experiments (Figures S1 and S2), we lowered this background by prephotobleaching a large region and then waiting 30 min for recovery (long enough for substantial return of the rapidly recovering fluorescence). As shown in Figure S1, under these conditions, the "mobile fraction" of Dpp fluorescence rises to about 75%. The fact that it does not rise to 100% indicates that original "immobile fraction" is not truly a static pool but simply one that recovers on a slow time scale. As described elsewhere (Supplemental Information), this behavior can be modeled by assuming that some internalized Dpp becomes transferred to a pool that degrades only very slowly (e.g., a long-lived vesicular compartment).

Numerical Solutions to Differential Equations

Systems of partial differential equations were solved using *Mathematica* software (Wolfram Research).

Supplemental Information

Supplemental Information includes five figures and Supplemental Experimental Procedures and can be found with this article online at doi:10.1016/j.cub.2012.02.065.

Acknowledgments

We thank Kavita Arora for helpful advice. Supported by NIH grants GM067247 and GM076516.

Received: October 4, 2011
Revised: January 9, 2012
Accepted: February 28, 2012
Published online: March 22, 2012

References

1. Crick, F.H.C. (1970). Diffusion in embryogenesis. Nature *225*, 420–422.
2. Lander, A.D., Nie, Q., and Wan, F.Y. (2002). Do morphogen gradients arise by diffusion? Dev. Cell *2*, 785–796.
3. Eldar, A., Dorfman, R., Weiss, D., Ashe, H., Shilo, B.Z., and Barkai, N. (2002). Robustness of the BMP morphogen gradient in *Drosophila* embryonic patterning. Nature *419*, 304–308.
4. Eldar, A., Rosin, D., Shilo, B.Z., and Barkai, N. (2003). Self-enhanced ligand degradation underlies robustness of morphogen gradients. Dev. Cell *5*, 635–646.
5. Mizutani, C.M., Nie, Q., Wan, F.Y., Zhang, Y.T., Vilmos, P., Sousa-Neves, R., Bier, E., Marsh, J.L., and Lander, A.D. (2005). Formation of the BMP activity gradient in the Drosophila embryo. Dev. Cell *8*, 915–924.
6. White, R.J., Nie, Q., Lander, A.D., and Schilling, T.F. (2007). Complex regulation of cyp26a1 creates a robust retinoic acid gradient in the zebrafish embryo. PLoS Biol. *5*, e304.
7. Nahmad, M., and Stathopoulos, A. (2009). Dynamic interpretation of hedgehog signaling in the Drosophila wing disc. PLoS Biol. *7*, e1000202.
8. Entchev, E.V., Schwabedissen, A., and González-Gaitán, M. (2000). Gradient formation of the TGF-beta homolog Dpp. Cell *103*, 981–991.
9. Kicheva, A., Pantazis, P., Bollenbach, T., Kalaidzidis, Y., Bittig, T., Jülicher, F., and González-Gaitán, M. (2007). Kinetics of morphogen gradient formation. Science *315*, 521–525.
10. Kruse, K., Pantazis, P., Bollenbach, T., Jülicher, F., and González-Gaitán, M. (2004). Dpp gradient formation by dynamin-dependent endocytosis: receptor trafficking and the diffusion model. Development *131*, 4843–4856.
11. Belenkaya, T.Y., Han, C., Yan, D., Opoka, R.J., Khodoun, M., Liu, H., and Lin, X. (2004). Drosophila Dpp morphogen movement is independent of dynamin-mediated endocytosis but regulated by the glypican members of heparan sulfate proteoglycans. Cell *119*, 231–244.
12. Bollenbach, T., Kruse, K., Pantazis, P., González-Gaitán, M., and Jülicher, F. (2007). Morphogen transport in epithelia. Phys. Rev. E Stat. Nonlin. Soft Matter Phys. *75*, 011901.
13. Wolpert, L. (2009). Diffusible gradients are out - an interview with Lewis Wolpert. Interviewed by Richardson, Michael K. Int. J. Dev. Biol. *53*, 659–662.
14. Hsiung, F., Ramirez-Weber, F.A., Iwaki, D.D., and Kornberg, T.B. (2005). Dependence of Drosophila wing imaginal disc cytonemes on Decapentaplegic. Nature *437*, 560–563.
15. Ramírez-Weber, F.A., and Kornberg, T.B. (1999). Cytonemes: cellular processes that project to the principal signaling center in Drosophila imaginal discs. Cell *97*, 599–607.
16. Schwank, G., Dalessi, S., Yang, S.F., Yagi, R., de Lachapelle, A.M., Affolter, M., Bergmann, S., and Basler, K. (2011). Formation of the long range Dpp morphogen gradient. PLoS Biol. *9*, e1001111.
17. Yu, S.R., Burkhardt, M., Nowak, M., Ries, J., Petrásek, Z., Scholpp, S., Schwille, P., and Brand, M. (2009). Fgf8 morphogen gradient forms by a source-sink mechanism with freely diffusing molecules. Nature *461*, 533–536.
18. Gregor, T., Wieschaus, E.F., McGregor, A.P., Bialek, W., and Tank, D.W. (2007). Stability and nuclear dynamics of the bicoid morphogen gradient. Cell *130*, 141–152.
19. Abu-Arish, A., Porcher, A., Czerwonka, A., Dostatni, N., and Fradin, C. (2010). High mobility of bicoid captured by fluorescence correlation spectroscopy: implication for the rapid establishment of its gradient. Biophys. J. *99*, L33–L35.
20. Castle, B.T., Howard, S.A., and Odde, D.J. (2011). Assessment of Transport Mechanisms Underlying the Bicoid Morphogen Gradient. Cell Mol Bioeng *4*, 116–121.
21. Schier, A.F., and Needleman, D. (2009). Developmental biology: Rise of the source-sink model. Nature *461*, 480–481.
22. Porcher, A., and Dostatni, N. (2010). The bicoid morphogen system. Curr. Biol. *20*, R249–R254.
23. Bollenbach, T., Pantazis, P., Kicheva, A., Bökel, C., González-Gaitán, M., and Jülicher, F. (2008). Precision of the Dpp gradient. Development *135*, 1137–1146.
24. Teleman, A.A., and Cohen, S.M. (2000). Dpp gradient formation in the Drosophila wing imaginal disc. Cell *103*, 971–980.
25. Lippincott-Schwartz, J., Altan-Bonnet, N., and Patterson, G.H. (2003). Photobleaching and photoactivation: following protein dynamics in living cells. Nat. Cell Biol. (*Suppl*), S7–S14.
26. Gurskaya, N.G., Verkhusha, V.V., Shcheglov, A.S., Staroverov, D.B., Chepurnykh, T.V., Fradkov, A.F., Lukyanov, S., and Lukyanov, K.A. (2006). Engineering of a monomeric green-to-red photoactivatable fluorescent protein induced by blue light. Nat. Biotechnol. *24*, 461–465.
27. Akiyama, T., Kamimura, K., Firkus, C., Takeo, S., Shimmi, O., and Nakato, H. (2008). Dally regulates Dpp morphogen gradient formation by stabilizing Dpp on the cell surface. Dev. Biol. *313*, 408–419.
28. Fujise, M., Takeo, S., Kamimura, K., Matsuo, T., Aigaki, T., Izumi, S., and Nakato, H. (2003). Dally regulates Dpp morphogen gradient formation in the Drosophila wing. Development *130*, 1515–1522.
29. Hinde, E., Cardarelli, F., Digman, M.A., and Gratton, E. (2010). In vivo pair correlation analysis of EGFP intranuclear diffusion reveals DNA-dependent molecular flow. Proc. Natl. Acad. Sci. USA *107*, 16560–16565.
30. Cardarelli, F., and Gratton, E. (2010). In vivo imaging of single-molecule translocation through nuclear pore complexes by pair correlation functions. PLoS ONE *5*, e10475.
31. Digman, M.A., and Gratton, E. (2009). Imaging barriers to diffusion by pair correlation functions. Biophys. J. *97*, 665–673.
32. Han, C., Belenkaya, T.Y., Khodoun, M., Tauchi, M., Lin, X., and Lin, X. (2004). Distinct and collaborative roles of Drosophila EXT family proteins in morphogen signalling and gradient formation. Development *131*, 1563–1575.
33. Takei, Y., Ozawa, Y., Sato, M., Watanabe, A., and Tabata, T. (2004). Three Drosophila EXT genes shape morphogen gradients through synthesis of heparan sulfate proteoglycans. Development *131*, 73–82.
34. Bornemann, D.J., Duncan, J.E., Staatz, W., Selleck, S., and Warrior, R. (2004). Abrogation of heparan sulfate synthesis in Drosophila disrupts the Wingless, Hedgehog and Decapentaplegic signaling pathways. Development *131*, 1927–1938.
35. Crickmore, M.A., and Mann, R.S. (2007). Hox control of morphogen mobility and organ development through regulation of glypican expression. Development *134*, 327–334.
36. Ohkawara, B., Iemura, S., ten Dijke, P., and Ueno, N. (2002). Action range of BMP is defined by its N-terminal basic amino acid core. Curr. Biol. *12*, 205–209.
37. Han, C., Belenkaya, T.Y., Wang, B., and Lin, X. (2004). Drosophila glypicans control the cell-to-cell movement of Hedgehog by a dynamin-independent process. Development *131*, 601–611.
38. Han, C., Yan, D., Belenkaya, T.Y., and Lin, X. (2005). Drosophila glypicans Dally and Dally-like shape the extracellular Wingless morphogen gradient in the wing disc. Development *132*, 667–679.
39. Gallet, A., Staccini-Lavenant, L., and Thérond, P.P. (2008). Cellular trafficking of the glypican Dally-like is required for full-strength Hedgehog signaling and wingless transcytosis. Dev. Cell *14*, 712–725.
40. Yan, D., and Lin, X. (2009). Shaping morphogen gradients by proteoglycans. Cold Spring Harb Perspect Biol *1*, a002493.
41. Umulis, D., O'Connor, M.B., and Blair, S.S. (2009). The extracellular regulation of bone morphogenetic protein signaling. Development *136*, 3715–3728.
42. Kuo, W.J., Digman, M.A., and Lander, A.D. (2010). Heparan sulfate acts as a bone morphogenetic protein coreceptor by facilitating ligand-induced receptor hetero-oligomerization. Mol. Biol. Cell *21*, 4028–4041.

43. Rusakov, D.A., and Kullmann, D.M. (1998). Geometric and viscous components of the tortuosity of the extracellular space in the brain. Proc. Natl. Acad. Sci. USA *95*, 8975–8980.
44. Olsen, S.K., Li, J.Y., Bromleigh, C., Eliseenkova, A.V., Ibrahimi, O.A., Lao, Z., Zhang, F., Linhardt, R.J., Joyner, A.L., and Mohammadi, M. (2006). Structural basis by which alternative splicing modulates the organizer activity of FGF8 in the brain. Genes Dev. *20*, 185–198.
45. Scholpp, S., and Brand, M. (2004). Endocytosis controls spreading and effective signaling range of Fgf8 protein. Curr. Biol. *14*, 1834–1841.
46. Pfeiffer, S., Ricardo, S., Manneville, J.B., Alexandre, C., and Vincent, J.P. (2002). Producing cells retain and recycle Wingless in Drosophila embryos. Curr. Biol. *12*, 957–962.
47. Bischof, J., Maeda, R.K., Hediger, M., Karch, F., and Basler, K. (2007). An optimized transgenesis system for Drosophila using germ-line-specific phiC31 integrases. Proc. Natl. Acad. Sci. USA *104*, 3312–3317.
48. Cullen, C.F., and Milner, M.J. (1991). Parameters of growth in primary cultures and cell lines established from Drosophila imaginal discs. Tissue Cell *23*, 29–39.